SI Appendix

Hip Extensor Mechanics and the Evolution of Walking and Climbing Capabilities in Humans, Apes, and Fossil Hominins

SI Text: Sensitivity Analyses

We performed sensitivity analyses to assess how robust results are to input parameter variation. DMA values (peak DMA and hip extension range) will be affected by: 1) sacral breadth 2) femur length 3) pelvic pitch, 4) the location of the origin of the hamstrings on the ischium, and 5) the location of hamstrings insertion on the tibia/fibula and knee flexion. Sensitivity analyses show that the pattern of results does not change over a wide range of plausible biological variation and/or measurement error in any of these variables.

1) Sacral Breadth: Sacral breadth is used to orient the pelves in the transverse plane under the assumption that the pubic symphysis lies at midline and the sacrum determines the inter-auricular distance and thus the spread of the posterior portion of the pelvis (SI Appendix, Fig. S3C). There are two possible sources of error in using the sacrum in this way. First, it is possible that in certain taxa the distance between the left and right superior auricular surface will be less than the maximum sacral breadth. There are no published data on the relationship between maximum sacral breadth and inter-auricular distance. Therefore, we address this possible source of error by calculating DMA envelopes with 100% to 80% maximum sacral breadth (SI Appendix, Table S4). This 20% is a wide and conservative range, much greater than the expected range of variation in inter-auricular distance in living species. In fossil taxa, reconstructions of specimens with various degrees of post-mortem damage impart a second potential source of error. For fossil specimens we examined DMA envelopes over a range of 90% to 110% reported maximum sacral breadth (SI Appendix, Tables S2 and S5).
2) Femur Length: Femur length is a proxy for B, the moment arm of the tangential force F_k produced at the knee in response to hamstrings force production (Fig. 1, SI Appendix Fig. S3). To address possible error in using this proxy, as well as estimated lengths in fossil taxa, we calculated DMA envelopes with femur lengths ±10% of measured (or estimated) length in both extant and fossil taxa (SI Appendix, Tables S2, S4, and S9).
3) Pelvic Pitch: For non-human primates, we estimated pelvic pitch based on mounted skeletons (SI Appendix, Table S11 and Fig. S7). Pelvic pitch also changes during locomotion. Based on published data in humans and chimpanzees pitch varies by approximately 10° (1). We therefore examined a range of ±10° in estimated pelvic pitch for both extant and fossil taxa (Figure 3; SI Appendix, Tables S4 and S9) to determine how variation in this variable affected DMA envelopes.
4) Hamstring Origin: The hamstrings originate on the ischial tuberosity. In our analyses, we use the midpoint of the most superior and to the most inferior points of the ischial tuberosity face as the origin point. However, the hamstrings originate throughout the ischial tuberosity, not only its center. We model the effect of hamstring origin point in SI Appendix Fig S2, using the most dorsal and ventral aspects of the ischial tuberosity to calculate a range of DMA envelopes.
5) Hamstring Insertion: The hamstrings insert on the proximal tibia and fibula distal to the knee joint rather than the distal femur. Thus, the exact location of the insertion site will vary for each muscle and as a function of knee flexion, and this variation will affect the moment arm, r, of the hamstrings. However, this effect is negligible, as modelled in SI Appendix Fig. S3, and will tend to amplify the difference in DMA envelopes between humans and non-human primates.

			Femur Length		Sacral Breadth		Ischium Length	
Taxon	**Sex**	**n**	**Mean**	**SD**	**Mean**	**SD**	**Mean**	**SD**
Homo sapiens	F	8	424	23	112	6	62	5
Homo sapiens	M	10	464	26	113	9	66	7
Pan troglodytes	F	4	291	14	70	7	72	5
Pan troglodytes	M	9	297	16	67	7	73	5
Pan troglodytes	U	7	289	19	70	6	72	7
Gorilla beringei	F	1	309	NA	83	NA	86	NA
Gorilla beringei	M	1	345	NA	124	NA	120	NA
Gorilla gorilla	F	5	299	17	85	6	80	5
Gorilla gorilla	M	7	349	13	93	8	106	5
Gorilla gorilla	U	4	345	26	95	12	100	13
Pongo abelii	F	5	250	6	67	4	56	3
Pongo pygmaeus	F	4	249	7	74	5	62	9
Pongo pygmaeus	M	8	264	12	80	10	66	6
Pongo pygmaeus	U	1	259	NA	70	NA	56	NA
Hylobates agilis	F	1	196	NA	42	NA	30	NA
Hylobates agilis	M	1	197	NA	34	NA	30	NA
Nomascus concolor	F	1	185	NA	38	NA	28	NA
Nomascus concolor	M	2	189	3	41	6	28	0
Hoolock hoolock	F	4	197	13	43	4	31	3
Hoolock hoolock	M	2	185	NA	38	NA	28	NA
Hylobates klossi	F	1	184	NA	39	NA	31	NA
Hylobates klossi	M	1	172	NA	33	NA	27	NA
Macaca fascicularis	F	3	124	5	34	3	27	1
Macaca fascicularis	M	1	137	NA	39	NA	30	NA
Macaca fascicularis	U	1	103	NA	31	NA	26	NA
Macaca mulatta	F	2	131	7	34	1	29	2
Mandrillus sphinx	F	2	212	7	48	1	41	1
Mandrillus sphinx	M	2	291	1	66	1	58	5
Papio hamadryas	M	2	244	31	71	1	51	4
Papio hamadryas	U	3	235	24	67	13	56	6
Colobus angolensis	F	1	185	NA	52	NA	32	NA
Colobus angolensis	M	2	201	8	48	1	36	0
Colobus guereza	F	3	173	26	45	10	30	6
Colobus guereza	M	3	204	14	54	4	38	4
Colobus guereza	U	1	171	NA	47	NA	30	NA
Procolobus badius	M	6	190	7	50	2	37	3
Ateles belzebuth	M	1	190	NA	51	NA	41	NA
Ateles fusciceps	F	1	202	NA	48	NA	35	NA
Ateles fusciceps	M	1	206	NA	53	NA	35	NA
Lagothrix lagotricha	F	4	155	11	38	5	25	2
Lagothrix lagotricha	M	1	147	NA	35	NA	27	NA
Alouatta seniculus	M	3	169	8	45	3	31	3
Cebus apella	F	1	138	NA	36	NA	24	NA
Cebus apella	M	6	129	6	40	2	28	2
Cebus olivaceus	F	1	147	NA	43	NA	28	NA
Cebus olivaceus	M	4	150	13	42	3	29	3

Table S1 | Extant Skeletal Sample. F, female; M, male; U, unknown sex. Femur length, sacral breadth, and ischial length in mm.

Specimen	Femur Length (±10% Range)	Sacral Breadth (±10% Range)
Ekembo nyanzae KNM-MW 13124 (2)	295 mm (266-325 mm)	65 mm (59-72 mm)
Ardipithecus ramidus ARA-VP 6/500 (3)	312 mm (281-343 mm)	105 mm (95-116 mm)
Australopithecus afarensis A.L. 288-1 (4)	281 mm (253-309 mm)	91 mm (82-100 mm)
Australopithecus africanus STS 14 (5)	276 mm (248-304 mm)	76 mm (68-84 mm)

Table S2 | Fossil Reconstructions. Includes the ±10% range used to account for reconstructed and/or worn specimens.

Taxon	DMA Envelopes					Passive Range		Locomotor Data							
	n	Max. DMA		Range		Min.	Max.	Condition	Kinematics		Kinetics				EMG
											Range		Max. Moment		
		Angle	Value	Min	Max.				Min.	Max.	Min	Max	Angle	Value	Range
Homo	18	141° (7°)	0.142 (0.02)	43° (6°)	223° (6°)	52° (9°)	200° (11°)	BLW	156° (4°)	200° (4°)	152°	193°	153°	0.16	~ 150° - 200°
Pan	20	85° (6°)	0.240 (0.01)	< 0°	162° (5°)	37° (11°)	159° (8°)	QLW *P.t.*	69° (4°)	103° (5°)	71°	105°	78°	1.17	~ 65° - 120°
								QLW *P.p.*	65° (9°)	115° (9°)	69°	104°	71°	0.56	
								QI 30° *P.p.*			52°	128°	50°	1.08	
								QI 45° *P.p.*			17°	84°	35°	1.12	~ 20° - 100°
								QI 60° *P.p.*			26°	96°	43°	0.98	
								VC *P.p.*	45° (11°)	131° (10°)	20°	92°	26°	0.37	~ 30° - 90°
Gorilla	18	76° (11°)	0.285 (0.03)	< 0°	150° (7°)	49° (4°)	150° (7°)	QLW	75° (4°)	120° (5°)					
								VC	52° (11°)	115° (11°)					
Pongo	18	86° (9°)	0.239 (0.03)	< 0°	163° (9°)	49° (8°)	164° (3°)	QLW	76° (8°)	108° (14°)					
								VC	27° (8°)	134° (21°)					
Hylobatidae	13	81° (7°)	0.154 (0.01)	< 0°	162° (7°)	26° (3°)	164° (12°)	BLW	105° (11°)	146° (9°)					
								VC	30° (19°)	110° (19°)					~ 30° -90°
Macaca sp.	7	97° (4°)	0.217 (0.01)	< 0°	176° (4°)	30° (4°)	150° (6°)	QLW	38° (11°)	117° (4°)					
Mandrillus	4	88° (6°)	0.192 (0.01)	< 0°	166° (6°)										
Papio	5	89° (5°)	0.218 (0.02)	< 0°	168° (6°)	37° (6°)	138° (14°)								
Colobus	10	95° (6°)	0.172 (0.01)	< 0°	172° (6°)	27°	158°								
Procolobus	6	87° (3°)	0.187 (0.01)	< 0°	166° (4°)										
Ateles	3	92° (3°)	0.184 (0.02)	< 0°	171° (3°)	29° (4°)	146° (12°)								
Lagothrix	5	89° (6°)	0.165 (0.01)	< 0°	168° (8°)										
Alouatta	3	90° (5°)	0.179 (0.01)	< 0°	168° (7°)										
Cebus	13	79° (6°)	0.203 (0.02)	< 0°	157° (5°)	27° (6°)	158° (17°)	BLW	~100°	~130°					

Table S3 | Hamstring DMA envelopes and comparative data. DMA Envelope: Means (standard deviations) for DMA ranges, angle of maximum DMA, and maximum DMA value. For some species, minimum extension (i.e., maximum hip flexion) is theoretically possible below 0°, which is not anatomically feasible *in vivo*. In those cases, minimum for the DMA range is given as <0°. **Passive Range**: Passive *in vivo* hip extension ranges in humans from (6); for non-human primates (pooled sexes) from (7). **Kinematics:** Minimum and maximum observed hip extension during quadrupedal walking on level ground (QLW) among zoo-housed *Pan troglodytes* (*P.t.*), *Pan paniscus* (*P.p.*), *Gorilla*, *Pongo*, and *Macaca*, from this study (Methods). Similar measures are taken from published figures for vertical climbing (VC, 8), and bipedal walking on level ground (BLW) in humans (9) and *Cebus* (10), and Hylobatidae (11). **Kinetics:** Range of hip extension (min.-max.) during which an extensor moment (i.e., torque) was measured via force plate. Maximum moment: peak dimensionless hip moment, scaled to body weight (N) and tibia length (m), and the angle at which peak moment occurs. **EMG:** Range of hip extension during which the hamstrings are active as assessed through electromyography (12-15).

	Min. Angle	Max. Angle	Angle, Max. DMA	Mean Max. DMA
Pelvic Pitch ±10°	***affected***	***affected***	***affected***	***no change***
Homo	43° (33°-43°)	223° (213°-233°)	141° (131°-151°)	0.14
Pan	< 0°	162° (152°-172°)	85° (75°-95°)	0.24
Gorilla	< 0°	150° (140°-160°)	76° (66°-86°)	0.29
Pongo	< 0°	163° (153°-173°)	86° (76°-96°)	0.24
Hylobatidae	< 0°	162° (152°-172°)	81° (71°-91°)	0.15
Macaca	< 0° (< 0°-6°)	176° (166°-186°)	97° (87°-107°)	0.22
Mandrillus sphinx	< 0°	166° (156°-176°)	88° (78°-98°)	0.19
Papio hamadryas	< 0°	168° (158°-178°)	89° (79°-99°)	0.22
Colobus	< 0° (< 0°-2°)	172° (162°-182°)	95° (85°-105°)	0.17
Procolobus badius	< 0°	166° (156°-176°)	87° (77°-97°)	0.19
Ateles	< 0° (< 0°-1°)	171° (161°-181°)	92° (82°-102°)	0.18
Lagothrix lagotricha	< 0°	168° (158°-178°)	89° (79°-99°)	0.17
Alouatta seniculus	< 0°	168° (158°-178°)	90° (80°-100°)	0.18
Cebus	< 0°	157° (145°-165°)	79° (69°-89°)	0.20
Sacral Breadth 100-80%	***affected***	***affected***	***affected***	***no change***
Homo	43°	223° (223°-225°)	141° (141°-144°)	0.14
Pan	< 0°	162° (162°-165°)	85° (85°-89°)	0.24
Gorilla	< 0°	150° (150°-154°)	76° (76°-81°)	0.29
Pongo	< 0°	163° (163°-166°)	86° (86°-90°)	0.24
Hylobatidae	< 0°	162° (162°-163°)	81° (81°-83°)	0.15
Macaca	< 0°	176° (176°-178°)	97° (97°-98°)	0.22
Mandrillus sphinx	< 0°	166° (166°-170°)	88° (88°-91°)	0.19
Papio hamadryas	< 0°	168° (168°-171°)	89° (89°-95°)	0.22
Colobus	< 0°	172° (172°-178°)	95° (95°-100°)	0.17
Procolobus badius	< 0°	166° (166°-170°)	87°(87°-90°)	0.19
Ateles	< 0°	171° (171°-173°)	92° (92°-95°)	0.18
Lagothrix lagotricha	< 0°	168° (168°-170°)	89° (89°-90°)	0.17
Alouatta seniculus	< 0°	168° (168°-173°)	90° (90°-92°)	0.18
Cebus	< 0°	157° (157°-161°)	79° (79°-83°)	0.20
Femur Length ±10%	***no change***	***no change***	***no change***	***affected***
Homo	43°	223°	141°	0.14 (0.13-0.14)
Pan	< 0°	162°	85°	0.24 (0.22-0.26)
Gorilla	< 0°	150°	76°	0.29 (0.26-0.32)
Pongo	< 0°	163°	86°	0.24 (0.22-0.26)
Hylobatidae	< 0°	162°	81°	0.15 (0.14-0.17)
Macaca	< 0°	176°	97°	0.22 (0.20-0.24)
Mandrillus sphinx	< 0°	166°	88°	0.19 (0.17-0.21)
Papio hamadryas	< 0°	168°	89°	0.22 (0.20-0.24)
Colobus	< 0°	172°	95°	0.17 (0.15-0.19)
Procolobus badius	< 0°	166°	87°	0.19 (0.17-0.21)
Ateles	< 0°	171°	92°	0.18 (0.17-0.20)
Lagothrix lagotricha	< 0°	168°	89°	0.17 (0.15-0.18)
Alouatta seniculus	< 0°	168°	90°	0.18 (0.16-0.20)
Cebus	< 0°	157°	79°	0.20 (0.16-0.22)

Table S4 | Sensitivity Analyses. Mean minimum and maximum hip angles at which DMA is >0 (where the hamstrings can produce a hip extension moment), as well as hip angle and DMA at peak DMA (where the hamstrings produce the highest moment for a unit of muscle force production) in extant taxa. Where angles are negative, indicating hip flexion past the trunk, angles are listed as < 0°. For each input parameter and variable, *affected* notes the variable varies as the parameter is changed; *no change* notes the variable does not vary as the parameter is changed.

Specimen	Orientation	Min. Angle	Max. Angle	Angle at Max DMA	Max. DMA
Ekembo nyanzae KNM-MW 13124 (2)	Quadruped	< 0°	120°-10°	50°-70°	0.204-0.251
Ardipithecus ramidus ARA-VP 6/500 (3)	Quadruped	< 0°	135°-160°	75°-95°	0.208-0.257
	Biped	15°-25°	195°-205°	125-135°	0.208-0.257
Australopithecus afarensis A.L. 288-1 (4)	Biped	20°-35°	200°-215°	130°-145°	0.138-0.173
Australopithecus africanus STS 14 (5)	Biped	< 0°-20°	180°-200°	110-130°	0.134-0.169

Table S5 | Fossil specimen hamstrings DMA envelopes characteristics.
Predicted minimum and maximum hip angles at which DMA is >0 (where the hamstrings would produce hip extension), as well as hip angle and DMA value at peak DMA (where the hamstrings would produce the highest moment for a unit of muscle force production) in fossil taxa. Where angles are negative, indicating hip flexion past the trunk, angles are listed as < 0°. Ranges indicate maximum and minimum values obtained using all combinations of input ranges: ±10% femur length, ±10% sacral breadth, ±10° pelvic pitch for non-bipedal orientation, and upper and lower bound pelvic pitch for bipedal orientations.

Number	Description	Type
1	**Posterior superior iliac spine**	**II**
2	Superior most point on iliac crest	III
3	**Anterior superior iliac spine**	**II**
4	**Anterior inferior iliac spine**	**II**
5	Superior acetabulum	III
6	Lateral acetabulum	III
7	Inferior acetabulum	III
8	Medial acetabulum	III
9	**Deepest point of acetabulum**	**II**
10	**Superior aspect of pubic symphysis**	**II**
11	**Inferior aspect of pubic symphysis**	**II**
12	Ischium at tip of tuberosity	II
13	**Most dorsal/inferior aspect of ischial tuberosity**	**II**
14	**Most dorsal/superior aspect of ischial tuberosity**	**II**
15	Inferior aspect of sciatic notch	II
16	Deepest point of sciatic notch	III
17	Superior aspect of sciatic notch	II
18	**Inferior aspect of auricular surface (where ala of sacrum articulates)**	**II**
19	**Superior aspect of auricular surface (where ala of sacrum articulates)**	**II**
20	Most superior point of obturator foramen	III
21	Most lateral point of obturator foramen	III
22	Most inferior point of obturator foramen	III
23	Most medial point of obturator foramen	III

Table S6 | Landmark set. Bolded landmarks were used in analyses. All other landmarks are only used for visualization purposes (SI Appendix, Figs. S1 and S3). Landmark type as defined by Bookstein (16).

Taxon	Angle
Gorilla	40°
Gorilla	38°
Pongo	42°
Pan (cast)	45°
Hylobates	41°
Papio	48°
Macaca	47°
Mandrillus (cast)	55°
Cebus	47°
Cebus	36°
Cebus	42°
Aotus	40°

Table S7 | Trunk Angles. Angles between the trunk axis (humeral head to greater trochanter) and the axis connecting the superior pubic symphysis and the ASIS in sagittal view (SI Appendix Fig. S7)

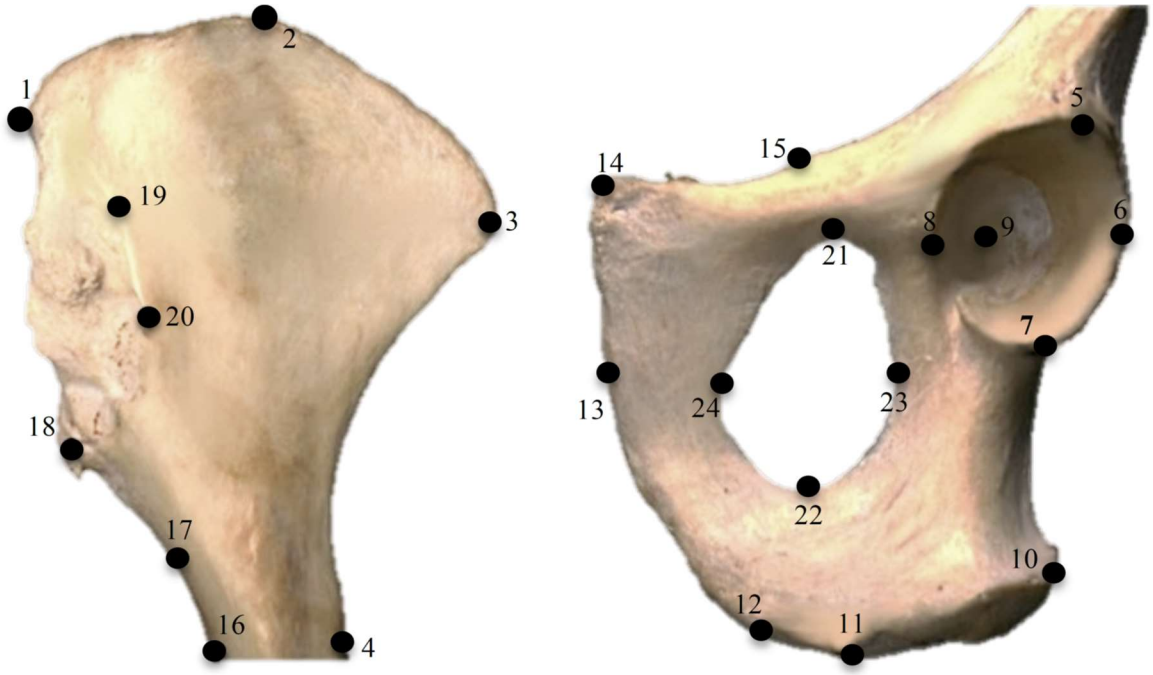

Figure S1 | Landmark Set. Left nonhuman primate os cox positioned in anterosuperior and anteroinferior orientations with landmarks as in SI Appendix Table S10 and Figure S6.

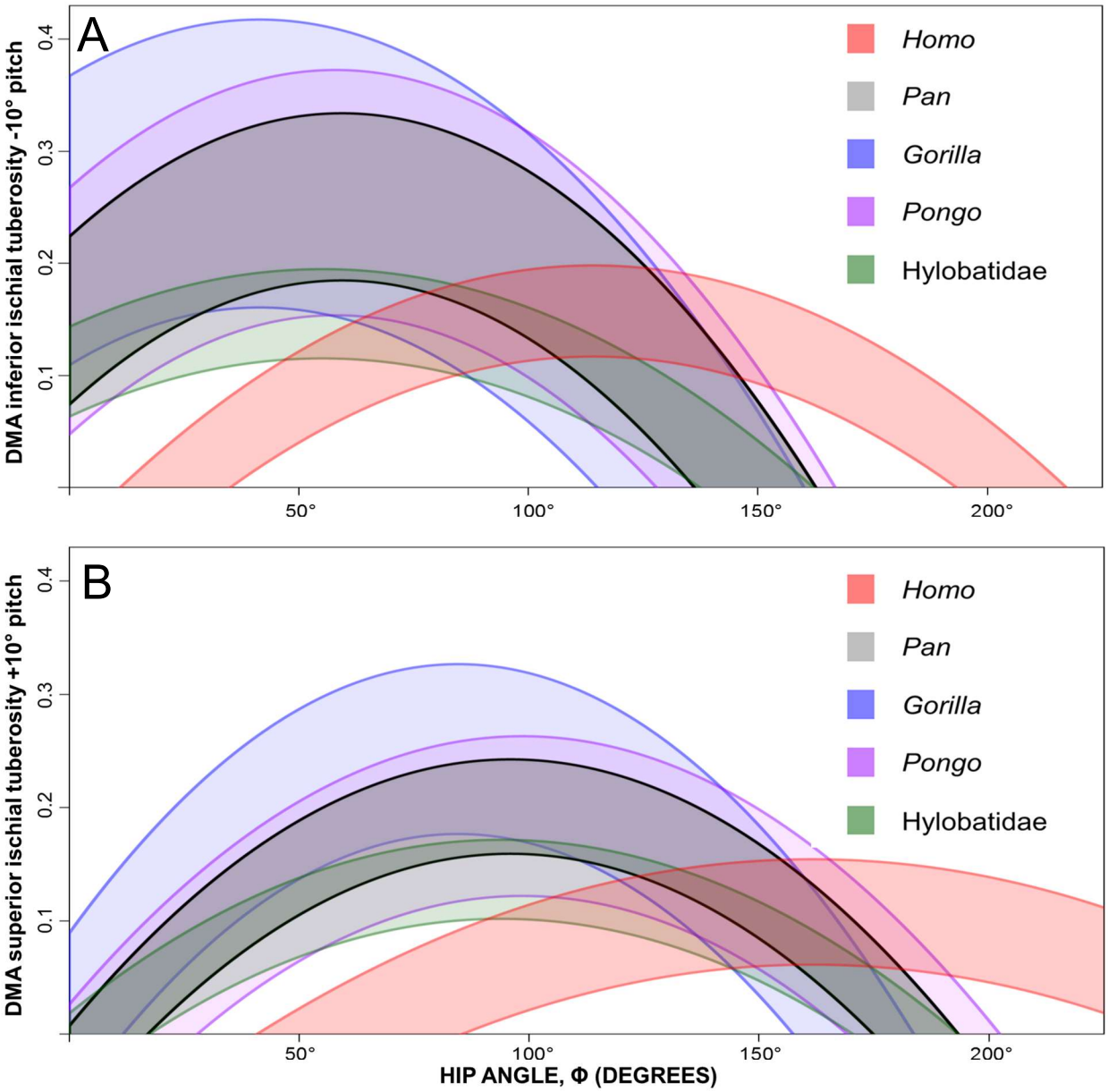

Figure S2 | Pelvic Pitch DMA Sensitivity Analysis (A) DMA modeled with hamstrings originating from the most inferior point of the ischial tuberosity and - 10° pelvic pitch. (B) DMA modeled with hamstrings originating from the most superior point of the ischial tuberosity and + 10° pelvic pitch. Shaded regions represent 95% prediction interval.

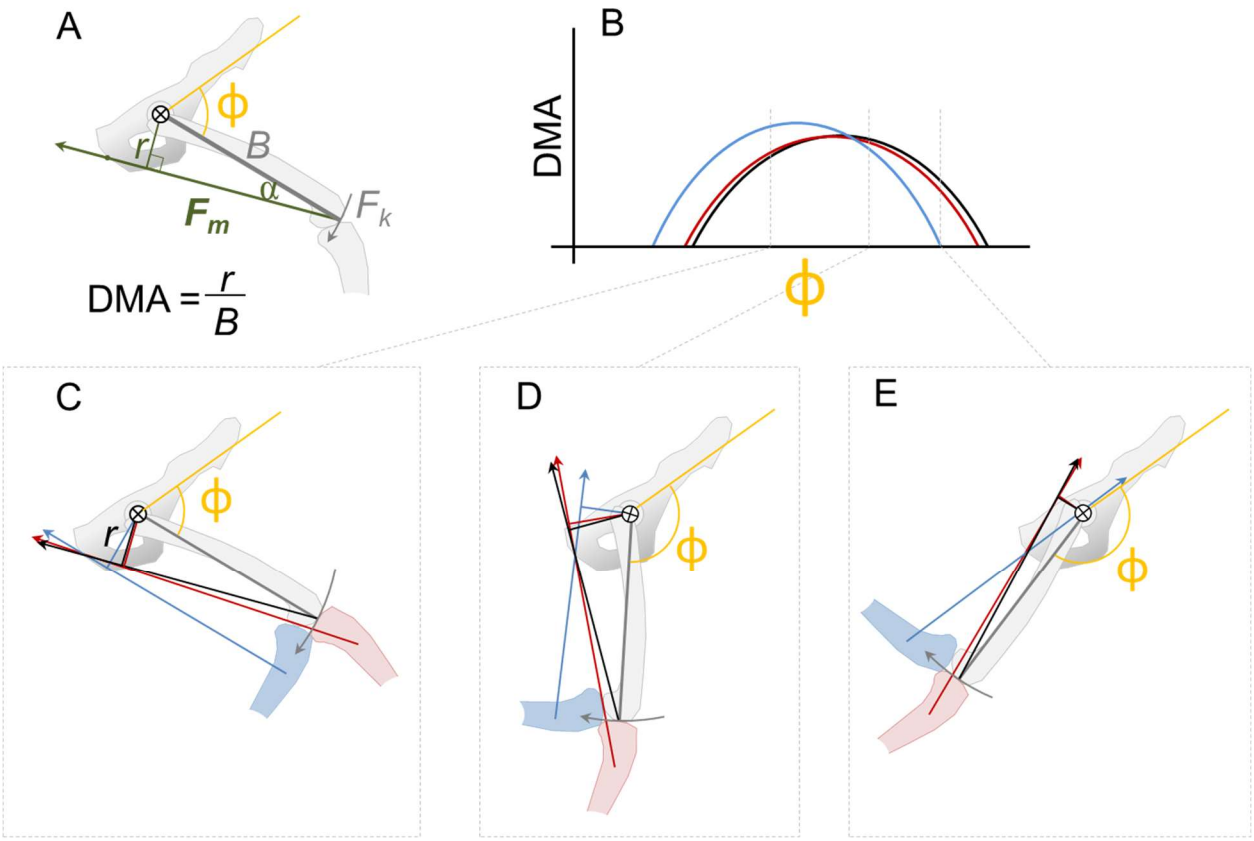

Figure S3 | Determining DMA and effects of hamstrings insertion. (A) The moment arm for the hamstrings muscles, r, is defined as the orthogonal distance between the force vector for the hamstrings, F_m, and the hip center of rotation. We used the hip center of rotation (the deepest point of the acetabulum), the distal femur, and the origin of the hamstrings on the ischium to define a triangle, and calculated angle α using the law of cosines. Moment arm r was then calculated for a range of hip angles, ϕ, as $r = \sin(\alpha)B$, where B is femur length. DMA is defined as r / B, and represents the amount of tangential force F_k at the knee per unit of muscle force F_m. (B) Plotting DMA against ϕ gives the DMA envelope. Our approach makes the simplifying assumption that the hamstrings attach at the distal femur, which is anatomically incorrect: the true attachments are on the proximal tibia and fibula. The magnitude of error imposed by this assumption is dependent on the degree of knee flexion. (B-E) When the knee is extended (red lines and tibia), the effect of the assumption on r and DMA is negligible. When the knee is flexed (blue lines and tibia), peak DMA will be greater but the DMA range will shift leftward, reaching DMA=0 at a lower degree of hip extension. Because humans use a more extended knee and apes use a more flexed knee when walking, our simplifying assumption regarding hamstrings attachment is conservative: apes are likely to have even more restricted ranges of hip extension relative to humans than is modeled in Figure 2. See SI Text 1 for sensitivity analyses of femur length, pelvic tilt, and sacral width.

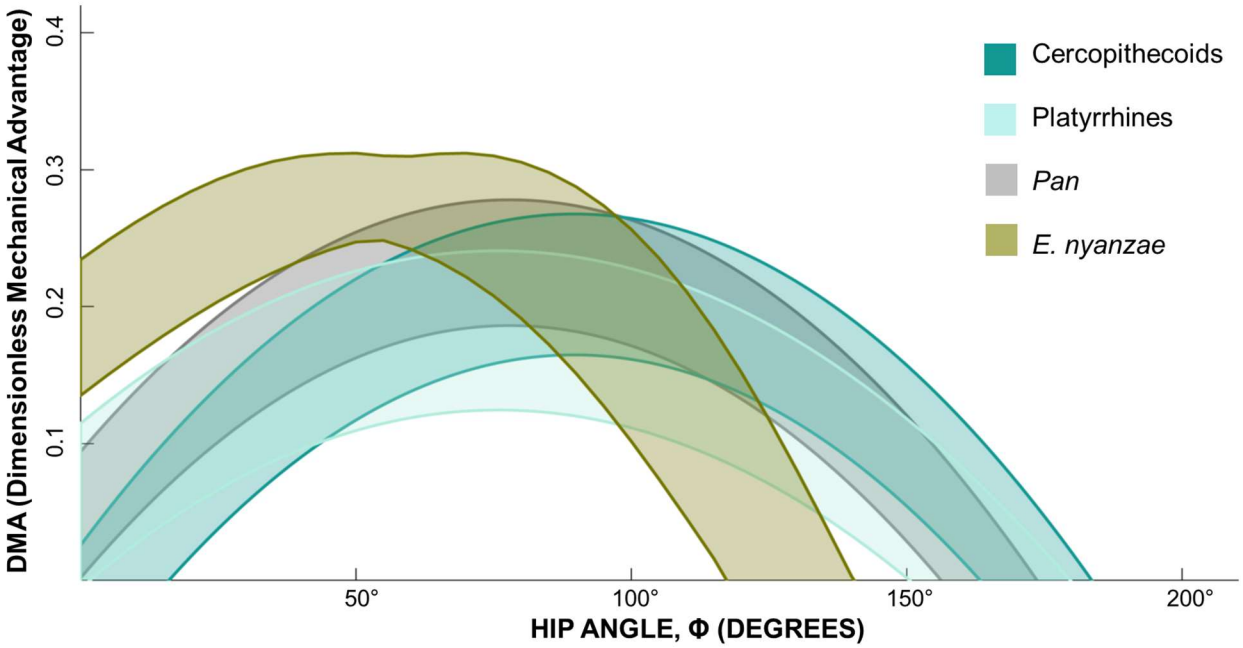

Figure S4 | Skeletally derived DMA in *Ekembo*. Shaded regions represent 95% prediction interval for cercopithecoids, platyrrhines, and chimpanzees. Shaded region for *Ekembo* includes ranges for pelvic pitch angle, sacral breadth, and femur length.

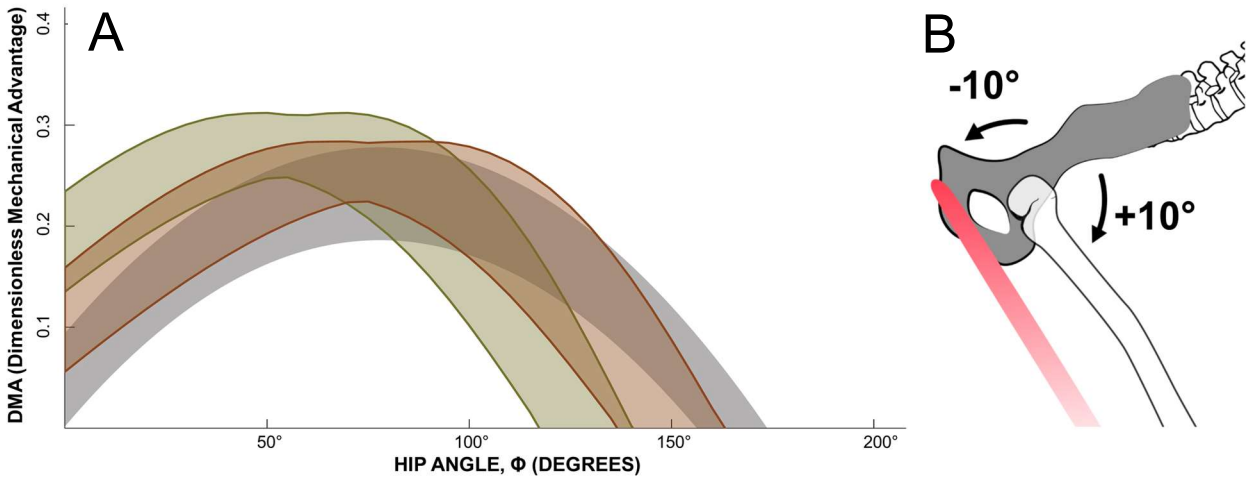

Figure S5 | Skeletally derived DMA in *Ardipithecus*, quadrupedal orientation. (A) Skeletally derived envelopes for hamstrings DMA; *Pan*, grey; *Ar. ramidus*, brown; *E. nyanzae*, green. Shaded region for *Pan* represents 95% prediction interval. Shaded regions for fossils represent range of pelvic pitch angles and reconstructed sacral breadths and femur lengths (see Methods). (B) The range of quadruped orientation in fossils is based on mounted skeletons of extant taxa (n=12) with ±10° to account for variation.

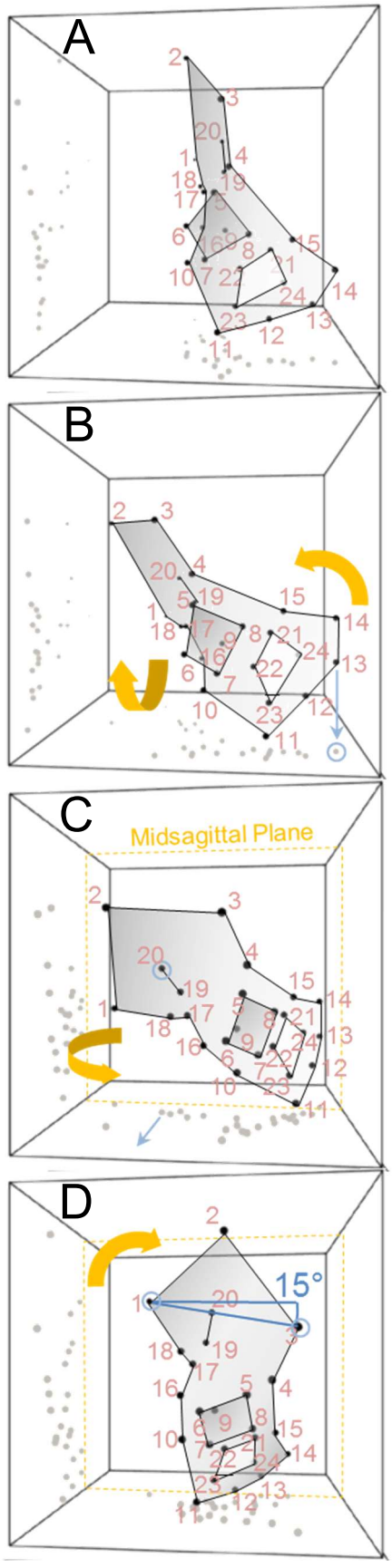

Figure S6 | Orientation of the ox coxae for analysis. Landmarks are numbered as in SI Appendix, Table S10 and shown for a human pelvis. Gray circles indicate reflected landmarks in the coronal (Z-Y) and transverse (X-Y) planes. (A) The superior pubic symphysis (landmark 14) was set at the origin (0,0,0). (B) Each pelvis was then rotated in the sagittal and coronal planes (orange arrows) such that the superior and inferior pubic symphyses (landmarks 13 and 14) were set at Y=0. Note that superior and inferior symphyses produce a single reflected point in the transverse plane (indicated with blue arrow and circle). (C) Specimens were then rotated in the transverse plane (orange arrow) so that the distance between the superior aspect of the auricular surface (landmark 20; blue circle, blue arrow on reflected point) and the mid-sagittal plane (orange dashed plane) was equal to half the sacral breadth. (D) Finally, the ox cox was rotated in the sagittal plane (orange arrow) to the appropriate degree of forward tilt. For humans, shown here, the segment (blue line) connecting the PSIS (landmark 1, blue circle) and ASIS (landmark 3, blue circle) reflected in the sagittal plane was oriented 15° relative to the X-axis, based on published anatomical dissections (17). For non-human primates, the pelvis was oriented such that the segment connecting the superior pubic symphysis (landmark 14) and ASIS was oriented -40° relative to the Z-axis, based on mounted skeletons (SI Appendix, Table S11 and Fig. S7). Fossil hominins (*Ardipithecus* and *Australopithecus*) were analyzed for a range of pelvic tilt, under the assumption that some portion of the medial gluteals must lie superior to the acetabulum to stabilize the trunk during single-leg stance. The most forward tilt, the posterior iliac spine (landmark 1) was oriented directly above the posterior acetabular margin (landmark 6). In the most backward tilt, the ASIS (landmark 3) was oriented directly above the anterior margin of the acetabulum (landmark 8). *Ekembo* was oriented as for non-human primates, and we also analyzed the *Ardipithecus* pelvis in this non-human primate orientation for a supplemental analysis (SI Appendix, Fig. S5). See SI Text 1 for sensitivity analyses regarding sacral width and pelvic tilt.

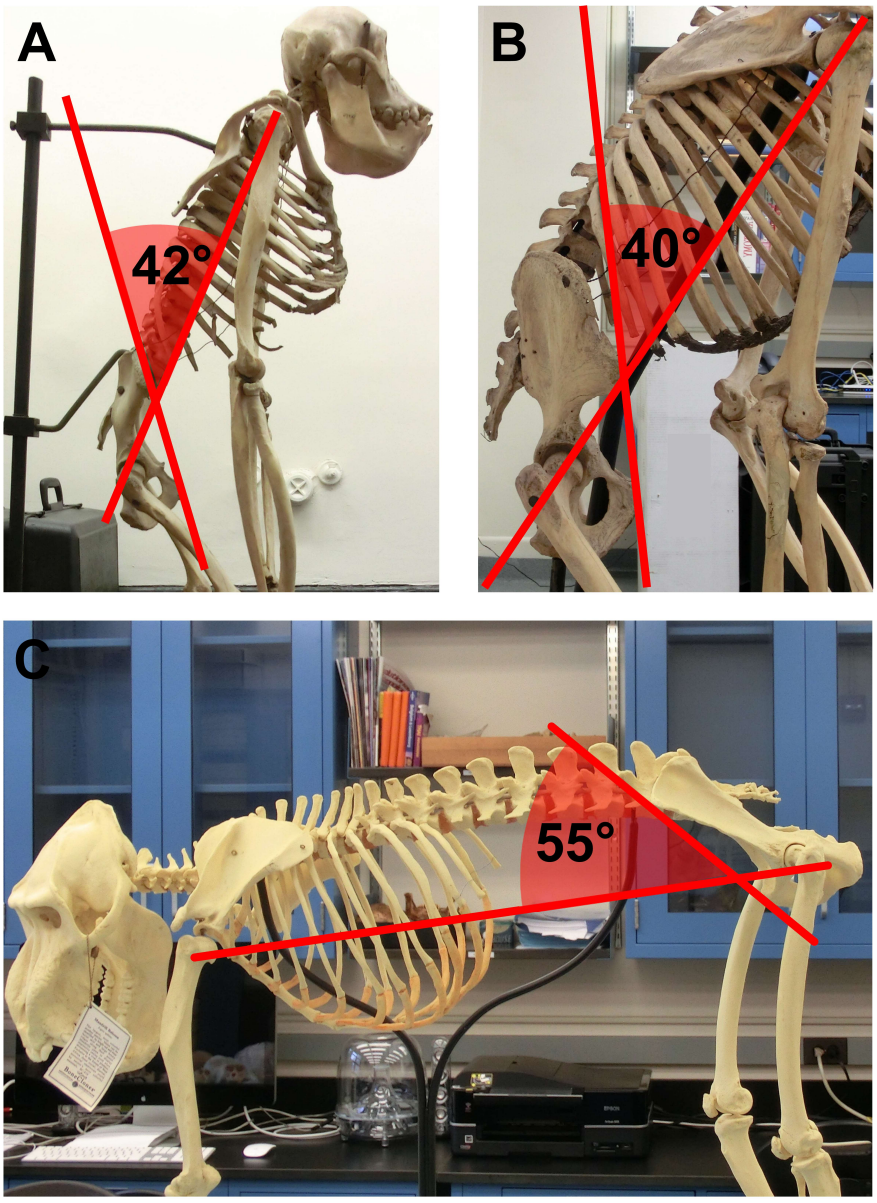

Figure S7 | Trunk Orientation. (A) *Pongo*, (B) *Gorilla*, (C) *Mandrillus* (cast). Lateral views showing angle between line connecting the superior pubic symphysis and ASIS and the line connecting the greater trochanter and humeral head.

SI References

1. O'Neill M, et al. (2015) Three-dimensional kinematics of the pelvis and hind limbs in chimpanzee (Pan troglodytes) and human bipedal walking. *J Hum Evol* 86:32-42.
2. Ward CV, Walker A, Teaford MF, Odhiambo I (1993) Partial skeleton of *Proconsul nyanzae* from Mfangano Island, Kenya. *Am J Phys Anthropol* **90**(1):77-111.
3. Lovejoy CO, Suwa G, Spurlock L, Asfaw B, White TD (2009) The pelvis and femur of *Ardipithecus ramidus*: the emergence of upright walking. *Science* **326**(5949):71e1–71e6.
4. Johanson DC, et al. (1982) Morphology of the Pliocene partial hominid skeleton (AL 288-1) from the Hadar formation, Ethiopia. *Am J Phys Anthropol* **57**(4):403-451.
5. Robinson JT (1972) Early Hominid Posture and Locomotion (Chicago Univ Press, Chicago).
6. Hallaçeli H, et al. (2014) Normal hip, knee and ankle range of motion in the Turkish population. *Acta Orthop Traumatol Turc* 48(1):37-42.
7. Hammond AS (2014) In vivo baseline measurements of hip joint range of motion in suspensory and nonsuspensory anthropoids. *Am J Phys Anthropol*. **153**(3):417-34.
8. Isler K (2005) 3D-kinematics of vertical climbing in hominoids. *Am J Phys Anthropol* **126**(1):66-81.
9. Kerrigan DC, Lee LW, Collins JJ, Riley PO, Lipsitz LA (2001) Reduced hip extension during walking: healthy elderly and fallers versus young adults. *Arch Phys Med Rehabil* 82(1):26-30.
10. Demes B (2011) Three-dimensional kinematics of capuchin monkey bipedalism *Am J Phys Anthro* 145(1):147-55.
11. Vereecke EE, D'Août K, Aerts P (2006) Speed modulation in hylobatid bipedalism: a kinematic analysis. *J Hum Evol* (5):513-26.

12. Larson SG, Stern JT (2009) Hip extensor EMG and forelimb/hind limb weight support asymmetry in primate quadrupeds. *Am J Phys Anthropol* **138**(3)343–355.
13. Kumakura H (1989) Functional analysis of the biceps femoris muscle during locomotor behavior in some primates. *Am J Phys Anthropol* **79**(3):379-391.
14. Benedetti MG, Agostini V, Knaflitz M, Bonato P (2012) Muscle activation patterns during level walking and stair ambulation. In *Applications of EMG in Clinical and Sports Medicine*. ed. Steele C (InTech, London), pp. 117-130.
15. D'Août K, Aerts P, De Clerq D, De Meester K, Van Esacker L (2002) Segment and joint angles of hind limb during bipedal and quadrupedal walking of the bonobo (*Pan paniscus*). *Am J Phys Anthropol* **119**(1):37-51
16. Bookstein FL (1991) *Morphometric tools for landmark data: Geometry and biology.* (Cambridge University Press).
17. Visser JJ, Hoogkamer JE, Bobbert MF, Huijing PA (1990) Length and moment arm of human leg muscles as a function of knee and hip-joint angles. *Eur J Appl Physiol Occup Physiol* 61(5-6):453-60.